Relationship between water retention capacity and pore-size distribution of compacted loess

Tao Xiao[1] · Ping Li[1,2] 🄳 · Zhenhui Pan[1] · Yifei Hou[1] · Jiading Wang[1]

Abstract

Purpose Different compaction conditions (i.e., molding water content or compaction degree is varied) can lead to great differences in the microstructure, which has a control on the mechanical and hydraulic properties of compacted loess. The effect of molding water content on both the microstructure and properties of compacted loess has been rarely reported. This study aims to gain a deep insight into the microstructure and water retention capacity of compacted loess under different compaction conditions.

Materials and method Compacted loess specimens with different molding water contents or compaction degrees were prepared, and their pore-size distribution curves (PSDs) and soil–water characteristic curves (SWCCs) were measured by various methods.

Results and discussion The pore-size distributions of small pores and mesopores are mainly affected by molding water content, while compaction degree only changes the density of mesopores in compacted loess. The influence of molding water content on the SWCC is mainly on the air-entry value (AEV) and slope of the curve in the transition zone, while compaction degree mainly influences the AEV.

Conclusions Molding water content has a control on the size of aggregates; with the increase of molding water content, the size of aggregates decreases, and the shape of PSD changes from bimodal to trimodal and then back to bimodal. The AEV corresponds to a diameter at which there is a sharp increase in the pore-size density. The slope of SWCC in the transition zone is related to the range of dominant diameter of inter-aggregate pores.

Keywords Compacted loess · Molding water content · Compaction degree · PSD · SWCC

✉ Ping Li
liping_dzxx@nwu.edu.cn

Tao Xiao
201921124@stumail.nwu.edu.cn

Zhenhui Pan
202021458@stumail.nwu.edu.cn

Yifei Hou
201932171@stumail.nwu.edu.cn

Jiading Wang
wangjd@nwu.edu.cn

[1] State Key Laboratory of Continental Dynamics, Department of Geology, Northwest University, Xi'an 710069, China

[2] Shaanxi Key Laboratory of Loess Mechanics and Engineering, Civil Engineering and Architecture Institute, Xi'an University of Technology, Xi'an 710048, China

1 Introduction

Loess, a type of quaternary aeolian sediment, is mainly distributed in arid and semi-arid regions, accounting for about 10% of the land area of the world (Li et al. 2016). The Loess Plateau of China has the most extensive and thickest loess deposition in the world; 70% of the loess in the world cumulates here (Derbyshire 2001; Li et al. 2016; Xu et al. 2021). Loess is featured by a high porosity, loose structure, and weak intergranular cementation. In particular, loess is highly sensitive to water. The geological disasters and geotechnical problems that are commonly seen in loess regions, such as landslide, mud flow, collapse, and ground subsidence, are generally related to water (Fan et al. 2017; Peng et al. 2018). In recent years, with the acceleration of urbanization in Northwest China, major engineering activities are unprecedentedly frequent in loess regions, such as the "Moving Mountains and Filling Gullies," "Smart City,"

and "Urban Subway Construction" project. In addition, the "Moving Mountains and Filling Gullies" project has become the main measure to add new construction land in the Loess Plateau. This measure not only makes the high-filling foundation become the main type of foundation (Zhu et al. 2019), but also changes the geological and hydrological equilibrium in local area (Li et al. 2019; Hou et al. 2020; Ge et al. 2021). For these reasons, increasing attention is drawn to the mechanical and hydraulic properties of compacted loess.

Both intact loess and compacted loess are typically unsaturated; their properties need to be defined as nonlinear unsaturated soil property functions (USPFs). The soil–water characteristic curve (SWCC) was found to hold an important relationship to each of the USPFs (Fredlund et al. 2012). In other words, the USPFs could be estimated from the SWCC, along with saturated soil properties (Vanapalli et al. 1996; Blatz et al. 2002; Al-Khazaali and Vanapalli 2019). Therefore, the SWCC, i.e., the relationship between water content and soil suction, is of great significance for addressing geotechnical problems related to unsaturated soils (Sun et al. 2016). Up to now, researches on the SWCC can be mainly divided into describing equations, influencing factors, measurement, estimation, description, and prediction of the hysteretic effect. The main factors influencing the SWCC are suggested to include the mineral composition, sample preparation conditions, temperature, and stress state and stress history (such as drying-wetting cycling and freezing–thawing cycling) (Aldaood et al. 2015; John et al. 2021). The sample preparation conditions of compacted soils mainly refer to molding water content, compaction degree (or dry density), and nature of energy (dynamic or static). When molded at different water contents, compacted soils may have very different properties even though they have identical dry densities, so it is difficult to duplicate an intact sample in the laboratory (Jiang et al. 2014; Wang et al. 2019; Hou et al. 2020). Different compaction conditions would result in great differences in the water retention capacity of compacted soils (Gallipoli et al. 2003; Ng et al. 2016; Wong et al. 2017; Zhang et al. 2021). Romero et al. (1999) found that compaction density can affect the SWCC in the low suction range. Jiang et al. (2017) reported that compaction density and water content influence the shape of SWCC. That is essentially due to the difference in soil structure; that is, the macro-mechanical and hydraulic properties of any soil are governed by its microstructure (Delage et al. 1996; Romero et al. 1999; Ng et al. 2016; Rabot et al. 2018; Li et al. 2020).

As mentioned, compaction degree and molding water content are the two factors controlling the microstructure of compacted soils when preparing specimens by static compaction in the laboratory. The effect of compaction degree (or dry density) is well studied and similar to that of confined compression (Wang et al. 2019). However, the effect of molding water content is not yet clear. It has been increasingly accepted that molding water content may change the type of structure (flocculated or dispersed) of compacted fine-grained soils (Vanapalli et al. 1999; Casini et al. 2012; Alonso et al. 2013). The effect of molding water content on both the microstructure and properties of compacted loess has been rarely studied. Guo et al. (2020) studied the effects of compaction density and water content on the permeability of compacted loess and suggested that the permeability is inversely proportional to either dry density or molding water content because the void ratio of compacted loess reduces as dry density or molding water content increases. Hou et al. (2020) compared the wetting SWCCs of loess samples molded at different water contents and observed that those SWCCs coincide when suction is greater than 70 kPa. In fact, molding water content is so important that not only the size and arrangement of skeleton particles but also the occurrence of clays and other cementing materials in compacted loess could be influenced by molding water content. For this reason, the effect of molding water content on the microstructure and water retention capacity of compacted loess is investigated in this study.

This study aims to (1) investigate the effects of molding water content and compaction degree on the pore-size distribution curve (PSD) and SWCC of compacted loess and (2) interpret the influence of microstructure on the water retention capacity of compacted loess. The results reveal the microstructure and water retention capacity of compacted loess under different compaction conditions, which can provide a helpful suggestion for the design and construction of artificial loess slopes and foundations, and are beneficial for the prevention of loess engineering hazards.

2 Material and methods

2.1 Test material

The loess tested was collected from Yan'an, China, at a depth between 4 and 6 m below the ground. The physical properties of the loess are summarized in Table 1, and the grain-size distribution curve shows that sands (> 0.075 mm), silts (0.002–0.075 mm), and clays (< 0.002 mm) take up

Table 1 Physical properties of the loess soil studied

Property	Value
In situ water content (%)	9.9
In situ density (g/cm^3)	1.46
Specific gravity, G_s	2.71
Liquid limit, w_L (%)	28.2
Plastic limit, w_P (%)	17.7
Plastic index, I_p	10.5

15.1%, 75.1%, and 9.8% by mass in the loess, respectively. The mineral composition was determined using the X-ray diffraction method. The minerals could be divided into non-clay minerals and clay minerals. Non-clay minerals include biotite, albite, quartz, and calcium carbonate. With regard to clay minerals, kaolinite was only identified. The compaction curve of the loess is shown in Fig. 1. It can be seen that the optimum water content is about 18%, and the maximum dry density is 1.75 g/cm^3.

2.2 Samples preparation

Compacted specimens were used in the tests, and the steps to prepare compacted specimens are as follows. Disturbed soils were first air-dried for several days, then crushed, and sieved using a 2-mm sieve. After that, the soils were oven-dried at a temperature of 105 ℃ and divided into five parts. Each part was added with a given amount of distilled water to achieve a predesigned gravimetric water content (14%, 16%, 18%, 20%, or 22%). The wet soils were sealed in plastic bags and stored in humid chambers for 72 h for water equalization. Thereafter, each soil was compacted statically using a self-designed sampling apparatus to a compaction degree of 85%, 90%, or 94%. In total, 15 groups of compacted loess specimens were prepared; they had different molding water contents or compaction degrees, as illustrated in Fig. 1. The properties of all compacted specimens are summarized in Table 2.

2.3 SWCC measurement

2.3.1 Axial translation technique

A 15-bar pressure plate extractor produced by the American Soil Moisture Instrument Company was used to
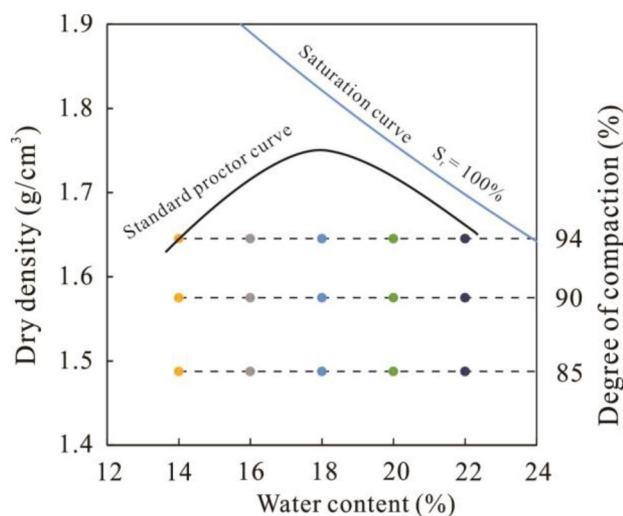
Table 2 Initial conditions of the compacted loess specimens tested

Specimen	MWC (%)	CD (%)	Dry density (g/cm^3)	Void ratio
14–85%	14	85	1.4875	0.8218
14–90%	14	90	1.5750	0.7206
14–94%	14	94	1.6450	0.6474
16–85%	16	85	1.4875	0.8218
16–90%	16	90	1.5750	0.7206
16–94%	16	94	1.6450	0.6474
18–85%	18	85	1.4875	0.8218
18–90%	18	90	1.5750	0.7206
18–94%	18	94	1.6450	0.6474
20–85%	20	85	1.4875	0.8218
20–90%	20	90	1.5750	0.7206
20–94%	20	94	1.6450	0.6474
22–85%	22	85	1.4875	0.8218
22–90%	22	90	1.5750	0.7206
22–94%	22	94	1.6450	0.6474

MWC molding water content, *CD* compaction degree

measure the SWCCs of compacted specimens in the low suction range (up to 1500 kPa). The specimens with a diameter of 5.3 cm and a height of 1 cm were saturated first and placed on the ceramic disk which was saturated in the pressure chamber. About 1.5 L distilled water was added to the chamber containing the ceramic disk, and an air pressure close to the air-entry value of the ceramic disk was applied to the chamber for 5 h. As water outflowed from the chamber at a constant rate, the ceramic disk was considered to be saturated. Then, an air pressure that could be controlled by the pressure control system was applied to the pressure chamber to obtain a predesigned suction (matric suction, equal to the air pressure applied to the specimens, i.e., axis translation technique) for drying the specimens. The air pressure applied to the specimens followed the order of $1 \rightarrow 3 \rightarrow 6 \rightarrow 9 \rightarrow 25 \rightarrow 50 \rightarrow 75 \rightarrow 100 \rightarrow 150 \rightarrow 200 \rightarrow 300 \rightarrow 400 \rightarrow 500 \rightarrow 700 \rightarrow 900 \rightarrow 1100$ kPa. In response to any suction increment, water would drain from the specimens until reaching the equilibrium. The equilibrium was considered to be reached when no water outflowing from the chamber. The time for the equilibrium varied between 4 and 14 days depending on the suction (or air pressure) applied to the specimens; the higher the suction, the more the time required for the equilibrium. This time in fact depends on the permeability of specimens, which in turn is controlled by the suction applied to the specimens (Schelle et al. 2013; Jiang et al. 2017; Zhang et al. 2021). After reaching the equilibrium, the specimens were taken out of the chamber and weighed for determining their water contents later.

Fig. 1 The compaction curve of the loess studied

2.3.2 Chilled-mirror dewpoint technique

The WP4C Dewpoint PotentiaMeter from METER Group was used to measure the suctions (total suction) greater than 1500 kPa since it has become acceptable practice to plot total suction when graphing SWCC in the high suction range (above 1500 kPa). This instrument can measure total suction using the chilled-mirror dewpoint technique in less than 20 min. The accuracy is $\pm$ 0.05 MPa in the range of 0–5 MPa and 1% in the range of 5–300 MPa. Previous studies have demonstrated the successful use of this instrument for total suction measurement (Patrick et al. 2007; Lipovetsky et al. 2020).

After the measurement of suction using the pressure plate extractor, some specimens were used to prepare specimens for the measurement of total suction using the WP4C. The specimen with a diameter of 4 cm filled about half the capacity of the container (1 cm high), which was then placed in a sealed chamber in the WP4C. The specimen would equilibrate with the water vapor in the chamber, which is equipped with a mirror whose temperature is precisely controlled by a thermoelectric cooler. Before each measurement, the 0.5 mol/kg KCl standard solution was used to calibrate the WP4C. After each measurement, the specimen was weighed and placed in a desiccator for drying for some time.

2.4 PSD measurement—MIP technique

The PSDs of compacted loess specimens were determined using the MIP technique, which is coming-of-age and has been commonly used to quantitatively characterize the pore structure of porous media (Juang et al. 1986; Romero et al. 1999; Jiang et al. 2014; Li et al. 2020; Xiao et al. 2022). The porosimeter used in this study could apply a pressure ranging between 0.5 and 60,000 psi to the mercury, and the corresponding range of entrance diameter was 3 nm–360 µm according to the law of capillarity. The specimens for the MIP tests were 1 cm $\times$ 1 cm $\times$ 1 cm in size and extracted from the specimens after the measurement of SWCC. Before each test, the specimen was dried using the freezing-drying method and placed in the chamber that was full of mercury in the porosimeter. The pressure in the mercury was subsequently raised in steps, causing the mercury to intrude the soil pores progressively, from the larger to the smaller.

3 Results and analysis

3.1 SWCCs of compacted loess specimens

The drying SWCC was determined using the axis translation and chilled-mirror dewpoint techniques. The curve was fitted with the equation proposed by van Genuchten (1980):

$$\theta = \theta_r + \frac{\theta_s - \theta_r}{[1 + (\alpha s)^n]^m} \tag{1}$$

where θ is the volumetric water content, %; θ_s is the saturated volumetric water content, %; θ_r is the residual volumetric water content, %; s is the suction, kPa; α is a fitting parameter primarily related to the inverse of air-entry value (AEV); n is a fitting parameter primarily related to the rate of water escaping from the soil once the AEV has been exceeded; and m is a fitting parameter primarily related to the residual water content (Fredlund et al. 2012). The desaturation of a soil is commonly divided into three stages, which are delineated by three zones on the drying SWCC, i.e., boundary effect zone, transition zone, and residual zone (Vanapalli et al. 1996). In the boundary effect zone with suctions up to the AEV, the soil is essentially saturated. In the transition zone that is between the AEV and residual suction, water content reduces significantly in response to suction increase. This is a two-phase zone; the continuity of water phase reduces while that of air phase grows. In the residual zone with suctions beyond the residual suction, large increases in suction lead to relatively small changes in water content, and the air phase gets continuous. The desaturation is dominated by the capillarity in the boundary effect zone and transition zone, in which suctions were measured using the pressure plate extractor, while the desaturation is controlled by the absorption in the residual zone, in which suctions were measured using the WP4C.

It is worth noting that the volume change that may occur due to drying was not considered when the measured gravimetric water content was converted into volumetric water content. That is because the drying-induced change in the PSD under null pressure condition was observed to be very small.

3.1.1 Effect of molding water content on the SWCC

The SWCCs of specimens compacted at different molding water contents are shown in terms of both volumetric water content (Fig. 2) and gravimetric water content (Fig. 3). It should be noted that the data of all specimens measured by WP4C are almost the same; so, only the data measured by pressure plate extractor are concerned. That is understandable since the adsorption that contributes to retaining water during the residual stage is dependent on the mineral composition, which is invariable among specimens.

It can be seen from Fig. 2 that the influence of molding water content is mainly on the AEV and slope of the curve in the transition zone. At the same compaction degree, the specimen with a lower molding water content has a greater AEV and a larger slope of the curve in the transition zone. So, for the specimens with the same compaction degree, their SWCCs intersect at a suction, below which the
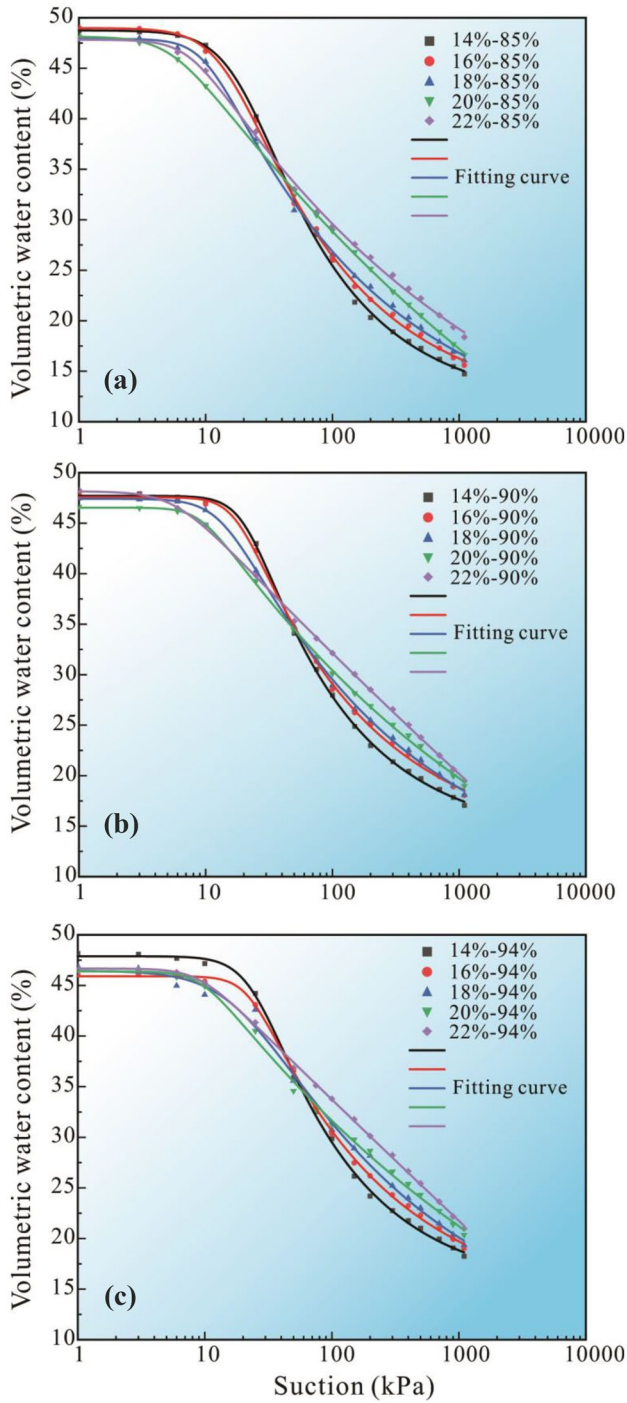
Fig. 2 SWCCs in terms of volumetric water content of the specimens compacted to compaction degrees of **a** 85%, **b** 90%, and **c** 94%

Fig. 3 SWCCs in terms of gravimetric water content of the specimens compacted to compaction degrees of **a** 85%, **b** 90%, and **c** 94%

specimen with a lower molding water content holds more water than the specimen with a larger molding water content at the same suction, while the opposite is true beyond this suction.
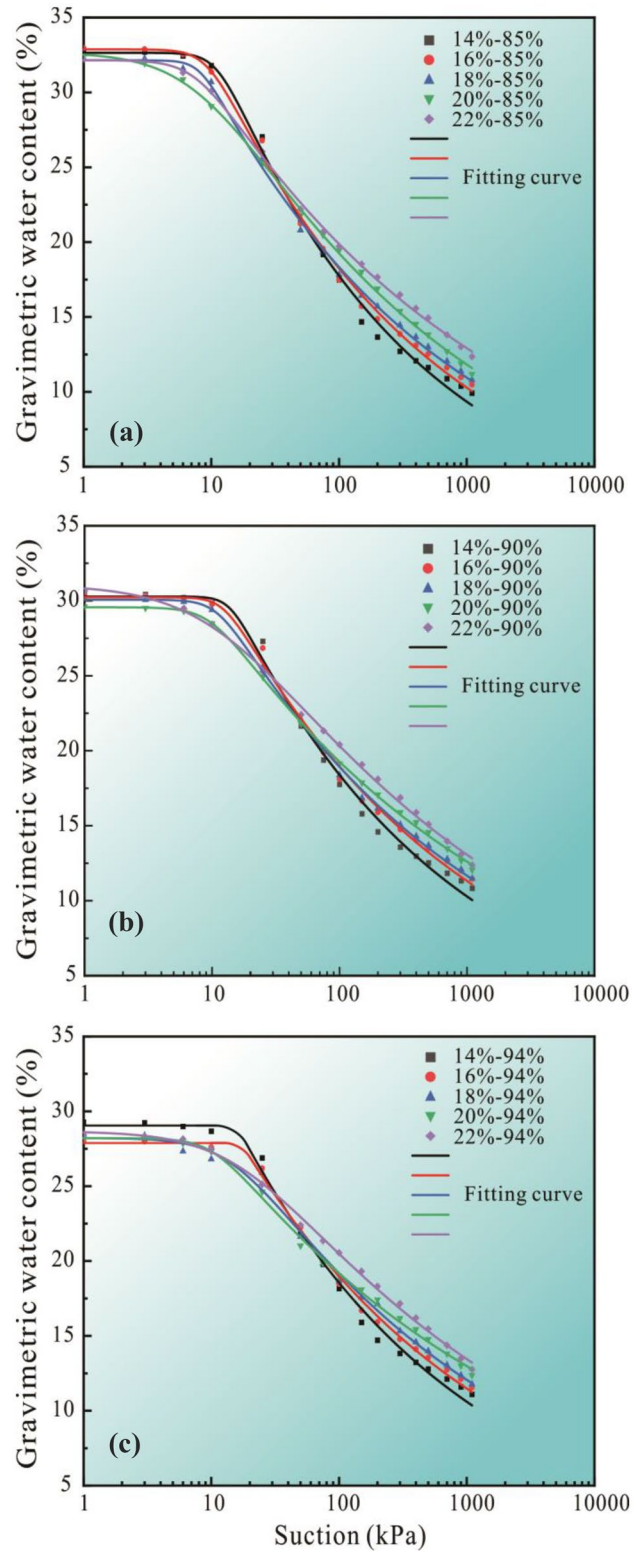
Table 3 Summary of the fitting parameters of the VG SWCC model

Specimen	α	m	n	R^2
14–85%	0.05289	0.2352	2.5143	0.9991
14–90%	0.0479	0.1403	3.9905	0.9994
14–94%	0.0412	0.1692	3.3976	0.9989
16–85%	0.0687	0.1769	2.6452	0.9990
16–90%	0.0573	0.1009	4.3200	0.9989
16–94%	0.0447	0.0947	4.3713	0.9992
18–85%	0.0997	0.0894	3.5968	0.9989
18–90%	0.0741	0.0923	3.2890	0.9991
18–94%	0.0545	0.1518	1.9016	0.9935
20–85%	0.1630	0.0377	2.7706	0.9997
20–90%	0.1097	0.0374	4.2337	0.9992
20–94%	0.1058	0.0356	3.8676	0.9969
22–85%	0.1764	0.0542	3.3383	0.9985
22–90%	0.1330	0.0099	2.8068	0.9994
22–94%	0.1132	0.0028	3.4915	0.9993

The SWCCs in terms of gravimetric water content are comparable to that in terms of volumetric water content. At the same compaction degree, the curves intersect at a suction, above which the curve of the specimen with a lower molding water content is below that of the specimen with a higher molding water content, meaning that the latter has a better water retention capacity than the former at the same suction. Similar results were obtained by Jiang et al. (2017) on compacted Lanzhou loess.

Table 3 summarizes the fitting parameters of the VG model for all compacted loess specimens. It can be seen

that the VG model provides an excellent representation of the measured curve, with a deviation parameter, R^2, greater than 0.99. As mentioned earlier, α is primarily related to the inverse of AEV. The variation of α with respect to molding water content and compaction degree is shown in Fig. 4a; α reduces with the increase of compaction degree that is because the AEV grows with the increase of compaction degree, as mentioned earlier. Shen et al. (2021) suggested a quadratic function of dry density for α based on their test results. It can be seen from Fig. 4b that at the same compaction degree, α grows almost linearly with the increase of molding water content. Moreover, the influence of molding water content on α gets less significant with the increase of compaction degree.

3.1.2 Effect of compaction degree on the SWCC

The SWCCs of specimens compacted to different compaction degrees are shown in terms of both volumetric water content (Fig. 5) and gravimetric water content (Fig. 6). Similarly, only the data measured by pressure plate extractor are concerned.

From Fig. 5, it can be seen that compaction degree has a significant influence on the SWCC of compacted loess, to be specific, the saturated water content and AEV. The saturated water content decreases with the increase of compaction degree, which is understandable. The AEV grows with the increase of compaction degree. For example, the AEVs of the specimens compacted at a water content of 14% to compaction degrees of 85%, 90%, and 94% are approximately 14, 18, and 19 kPa, respectively (Fig. 5a). That is because the
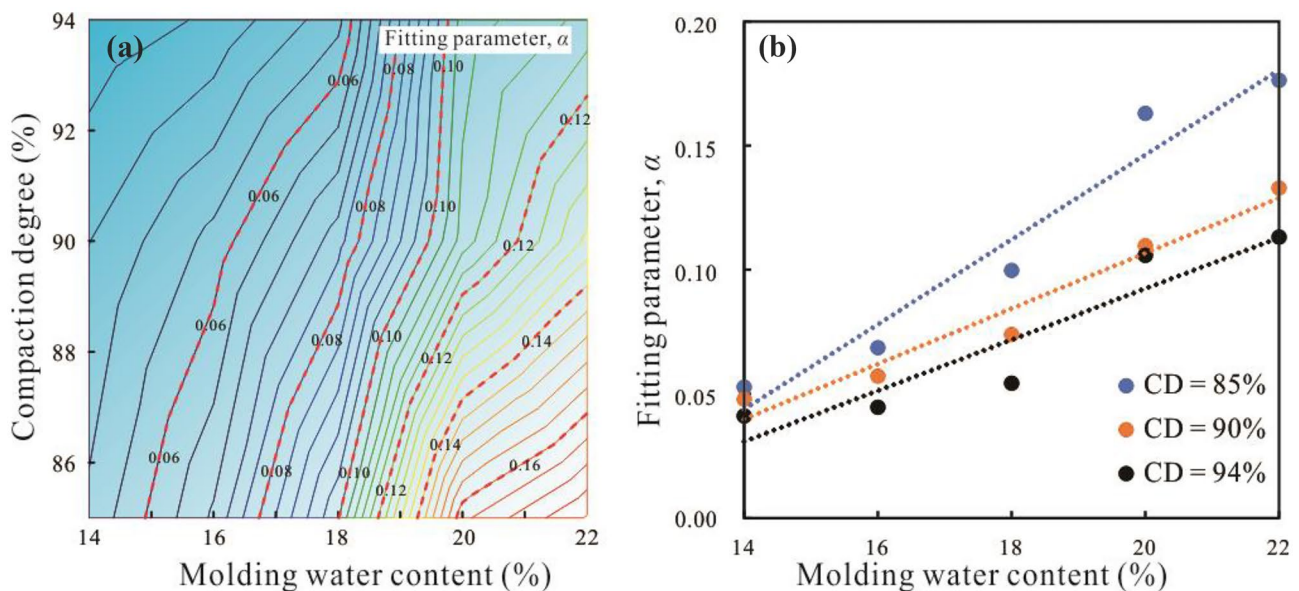
Fig. 4 Variation of the fitting parameter α with respect to molding water content and compaction degree (CD means compaction degree)

Fig. 5 SWCCs in terms of volumetric water content of the specimens compacted at water contents of **a** 14%, **b** 16%, **c** 18%, **d** 20%, and **e** 22%
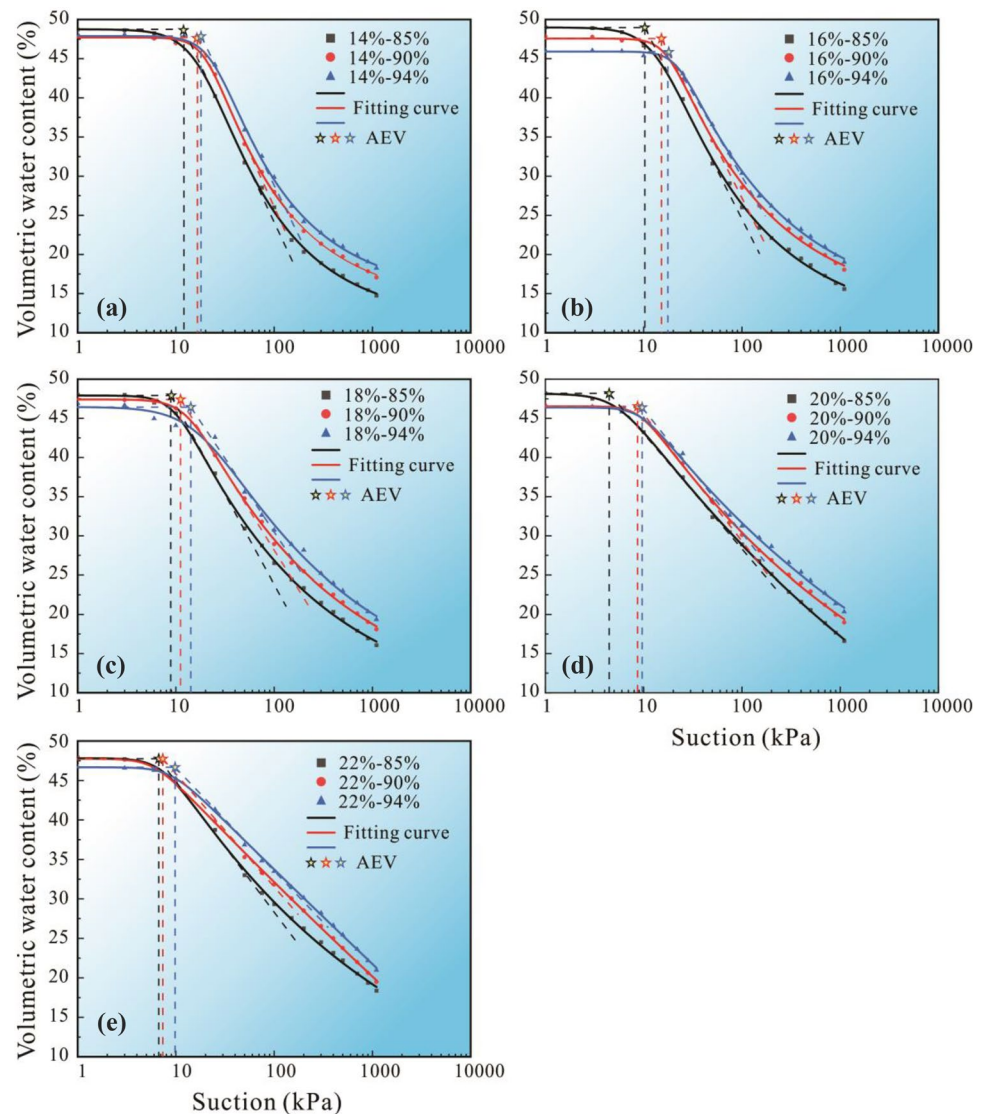
AEV is the suction at which air enters the largest pores in the soil; it therefore relates to the maximum diameter of pores in the soil (Vanapalli et al. 1996). The maximum diameter of pores in compacted loess is linearly related to compaction degree, reported by Wang et al. (2019). For these reasons, at the same molding water content, the curves of the specimens with different compaction degrees intersect at a suction around the AEV. Besides, the SWCCs in terms of volumetric water content are very different in the transition zone.

As the SWCCs are presented in terms of gravimetric water content, the effect of compaction degree on the saturated water content is magnified, see Fig. 6. In comparison to the SWCCs in terms of volumetric water content, the curves in terms of gravimetric water content are almost overlapped when suction is approximately greater than 30 kPa. Similar result was observed by Hou et al. (2020), who measured the wetting SWCCs of compacted loess specimens using

the filter paper method. Their specimens were remolded at a water content of 10% to different dry densities (i.e., 1.5, 1.6 and 1.7 g/cm^3). They suggested that compaction density and disturbance to the intact structure have no impact on the SWCC in the suction range of 10^2–10^5 kPa.

3.2 PSDs of compacted loess specimens

3.2.1 Effect of molding water content on the PSD

Figure 7 shows the PSDs of specimens compacted at different molding water contents. It can be seen that, except for the specimens compacted at the water content of 22%, all the other PSDs display a bimodal characteristic, suggesting that there are two families of pores in the specimens. That is because aggregates which are associations of elementary particles (sands, silts and clays) are skeleton particles in compacted loess. Each aggregate (both clay

Fig. 6 SWCCs in terms of gravimetric water content of the specimens compacted at water contents of **a** 14%, **b** 16%, **c** 18%, **d** 20%, and **e** 22%
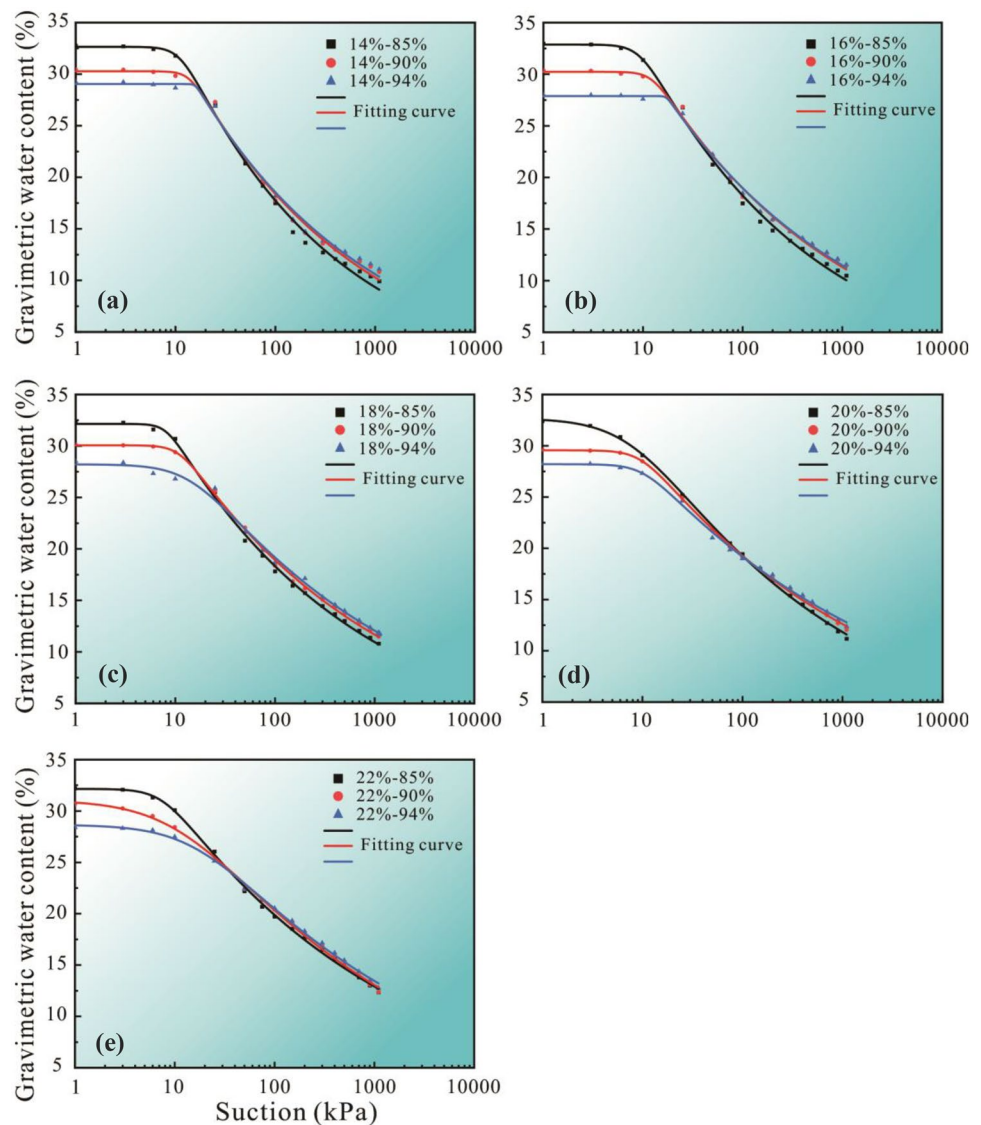
aggregates and silt–clay aggregates, the latter is hereinafter shortened to silt aggregates) has its microstructure, while aggregates are arranged to form the skeleton structure of compacted loess. The pores in aggregates belong to the family of intra-aggregate pores, and the pores between aggregates belong to the family of inter-aggregate pores. According to the idealized PSD proposed by Xiao et al. (2022) for compacted loess, the boundary diameter of the two pore families is about 150 nm.

It is shown in Fig. 7 that the size distribution of intra-aggregate pores is not affected by molding water content at any compaction degree, as indicated by the overlapping curves in the diameter range of intra-aggregate pores. With the increase of molding water content, the peak density (corresponding to the dominant diameter) of inter-aggregate pores reduces greatly, whereas the dominant diameter of inter-aggregate pores (d_{macro}) changes a little. Besides, as

molding water content increases to 22%, the shape of PSD changes, from bimodal to trimodal. It indicates that molding water content might have a control on the shape of PSD of compacted loess, which will be discussed later.

To facilitate the description of PSD variation due to changes in molding water content, pores in compacted loess are classified into four groups: micropore ($d \leq 150$ nm), small pore (150 nm $< d \leq 2000$ nm), mesopore (2000 nm $< d \leq 12,000$ nm), and macropore ($d > 12,000$ nm) (see Fig. 7). Micro pores are in fact intra-aggregates, which are not affected. There is a number of macropores in the specimen 22–85% (molding water content-compaction degree), while the others almost have no macropores. At any compaction degree, the PSDs in the ranges of small pores and mesopores are mainly different. The larger the molding water content, the higher the density of small pores and the lower the density of mesopores (see Fig. 7). This can be seen
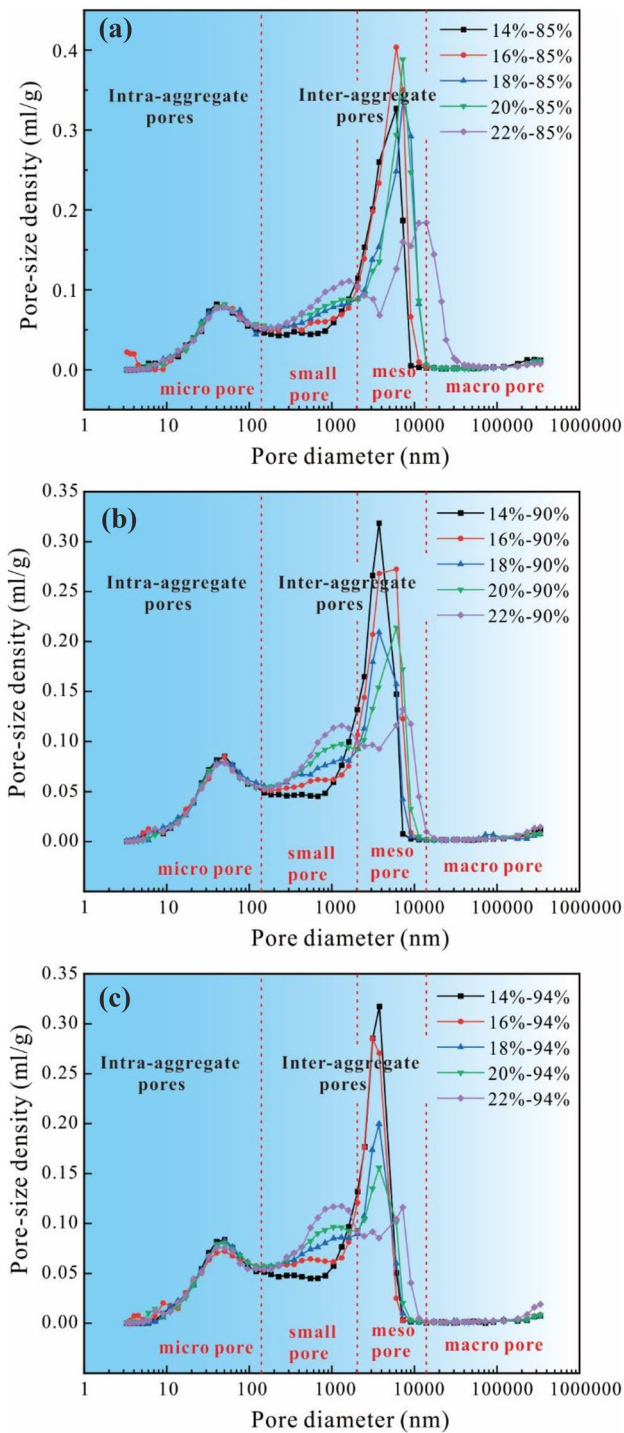
Fig. 7 PSDs of the specimens compacted to compaction degrees of **a** 85%, **b** 90%, and **c** 94%
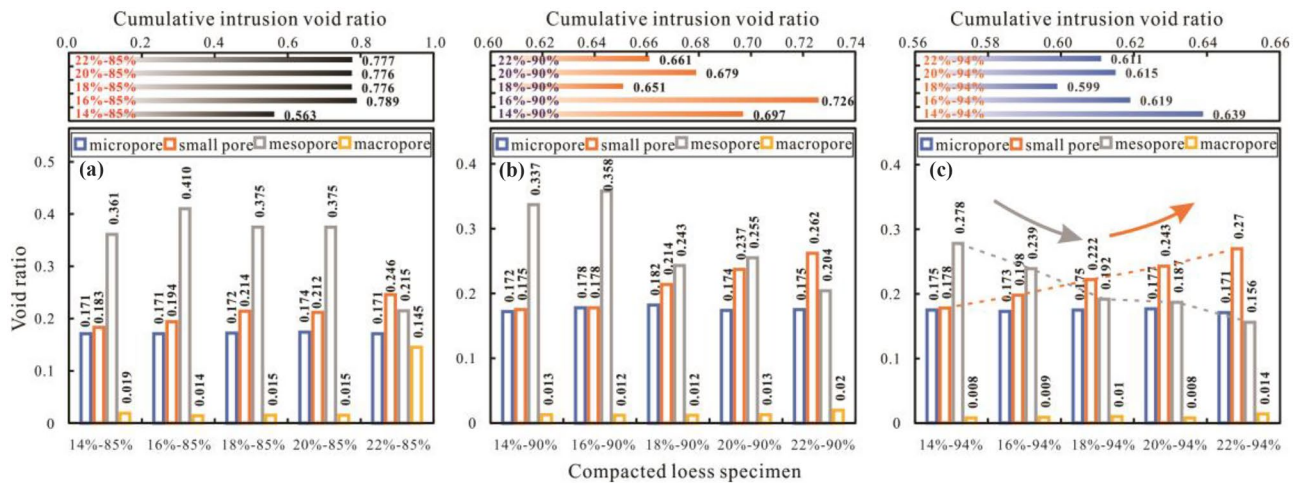
more clearly in Fig. 8, where the void ratios of micropores, small pores, mesopores, and macropores of specimens compacted at different molding water contents are compared. It

shows that the void ratio of small pores grows and the void ratio of mesopores reduces with the increase of molding water content at any compaction degree, while little changes take place in the void ratios of micropores and macropores. The cumulative intrusion void ratios (e_{in}) are also summarized in Fig. 8. The specimens with the same compaction degree should have identical void ratios (e), while different values of e_{in} were measured by MIP, which could be mainly because they have different PSDs. In general, e_{in} is less than e (as summarized in Table 2), because in addition to the pores with a diameter beyond the range of 3 nm–360 μm, insolated pores and constricted pores could not be intruded (Wang et al. 2020; Li et al. 2020; Xiao et al. 2022).

3.2.2 Effect of compaction degree on the PSD

Figure 9 shows the PSDs of specimens compacted to different compaction degrees. The PSDs of the specimens compacted at 22% are trimodal (Fig. 9e), and the others are bimodal, as mentioned before. In each group of specimens (with the same molding water content), the size distribution of intra-aggregate pores is not affected, while the PSD in the range of inter-aggregate pores is compressed towards the left as compaction degree increases. This differs from the assumption of Hu et al. (2013) and Zhang et al. (2019) that the PSD of inter-aggregate pores translates towards the left in response to the decrease of void ratio. Moreover, not only is the peak density of inter-aggregate pores decreased significantly, but also d_{macro} reduces.

Similarly, pores are classified into four groups (see Fig. 9). It can be seen that mesopores are mainly affected by compaction degree; the larger the compaction degree, the lower the density of mesopores. The PSD in the ranges of the other three groups of pores is basically unchanged. In fact, the specimen with a larger compaction degree is equivalent to be obtained by compressing the specimen with a lower compaction degree in a confined cell. So, the effect of compaction degree is similar to that of confined compression on the PSD of compacted loess, i.e., inter-aggregate pores are compressed, from the larger to the smaller, resulting in reductions in the peak density and dominant diameter of inter-aggregate pores (Wang et al. 2019). Figure 10 compares the void ratios of micropores, small pores, mesopores, and macropores, as well as e_{in}, of specimens compacted to different compaction degrees. It can be seen that at any molding water content, the void ratio of mesopores drops greatly with the increase of compaction degree, and the void ratios of the other three groups of pores remain basically unchanged. As a result, e_{in} that is the sum of the four void ratios decreases with the growing compaction degree.
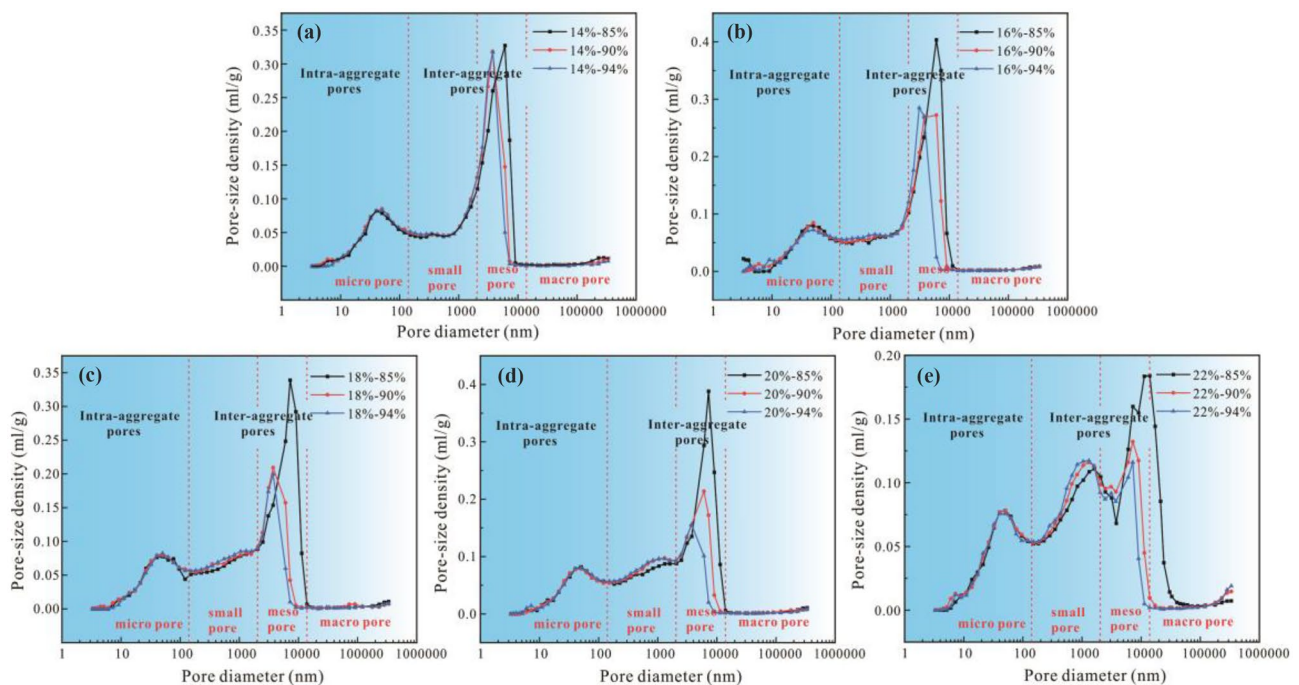
Fig. 8 Void ratios of micropores, small pores, mesopores, and macropores of the specimens compacted to compaction degrees of **a** 85%, **b** 90%, and **c** 94%

4 Discussion

4.1 Controlling effect of molding water content on the shape of PSD

As analyzed before, the size distributions of small pores (150 nm $< d \leq$ 2000 nm) and mesopores (2000 nm $< d \leq$ 12,000 nm) are mainly different in specimens with different molding water contents even if their compaction degrees are the same (Fig. 7). At the same compaction

degree, the larger the molding water content, the higher the density (or void ratio) of small pores, and the lower the density (or void ratio) of mesopores (Fig. 8). That is because molding water content has a significant influence on the size of skeleton particles (aggregates) in compacted loess. At a low molding water content, the diffuse double layer (DDL), i.e., water molecules electrically attracted to the surfaces of clay particles, could not be developed completely, such that attractions (such as van der Waals attraction and capillary attraction) are dominated between clay particles. Under such

Fig. 9 PSDs of the specimens compacted at water contents of **a** 14%, **b** 16%, **c** 18%, **d** 20%, and **e** 22%
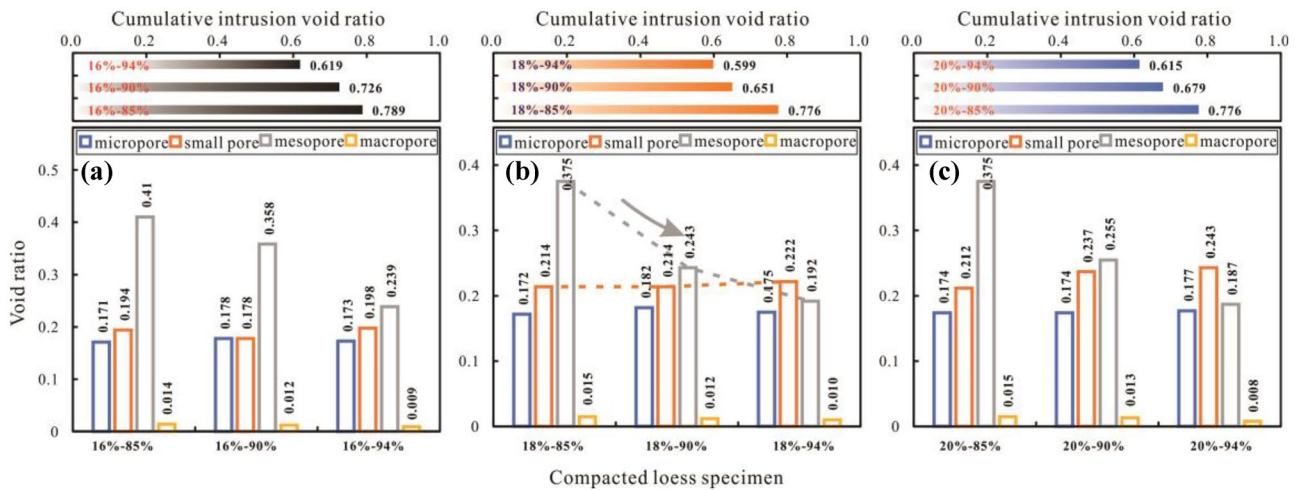
Fig. 10 Void ratios of micropores, small pores, mesopores, macropores, and e_{in} of the specimens compacted at water contents of **a** 16%, **b** 18%, and **c** 20%

a scenario, aggregates (both clay aggregates and silt aggregates) developed in compacted loess are more likely to have large sizes; pores between aggregates also have large sizes. While at a high molding water content, both aggregates and pores between aggregates have small sizes. For this reason, with the increase of molding water content, the density of small pores grows and the density of mesopores reduces.

Among the specimens tested in this study, only the specimen 22–85% has a number of macropores (Fig. 7a), while the others almost have no macropores. In addition, the PSDs of the specimens compacted at 22% are trimodal (Fig. 9e). Those curves have two peaks within the range of inter-aggregate pores ($d > 150$ nm). That is to say, there are two groups of inter-aggregate pores in those specimens. It suggests that molding water content may have a control on the shape of PSD of compacted loess. Delage et al. (1996) were among the first to interpret the PSD shape of compacted soils. Their results show that the specimen compacted at the wet side (higher than the optimum water content) had a matrix type structure along with a unimodal PSD, whereas the specimen compacted at the dry side had a bimodal PSD and a structure characterized by a skeleton made of silt aggregates linked together by clay bridges. Similar results were obtained by Kong et al. (2011) on a compacted clay, and they thought there is a reduction in the aggregation of clays in response to an increase in molding water content (Delage et al. 1996; Romero et al. 2011; Cheng et al. 2020). Casini et al. (2012) drew a very different conclusion based on their results on a compacted silt. They observed that aggregates could not be fully developed, in both the size and the quantity, when molding water content and compaction degree were all very low. In that case, the compacted silt had a unimodal PSD. While there was a high tendency for the development of aggregates when molding

water content was close to the optimum water content, the PSD turned to be bimodal. As molding water content increased further (the soil was nearly saturated), large pores were filled with aggregates, and the compacted silt had a unimodal PSD again. However, Koliji et al. (2009) reported different finding that the PSD of a silty clay was bimodal when it was compacted at low water contents, while as it went to be saturated (saturation degree > 50%), large pores were reduced, resulting in a unimodal PSD. These different findings could be mainly attributed to the differences in grain composition of the test materials and methods to determine the PSDs. For example, the peak in the diameter range of intra-aggregate pores (less than 200 nm, typically) could not be detected by MIP when the porosimeter used cannot provide a wide range of pressure (Casini et al. 2012; Hou et al. 2020; Wang et al. 2020; Cheng et al. 2020).

In the present study, the PSD of compacted loess is observed to vary from bimodal to trimodal as molding water content increases from 14 to 22%. To investigate in depth the controlling effect of molding water content on the shape of PSD of compacted loess, five more specimens were prepared, and their PSDs were measured, as shown in Fig. 11. They were compacted at 8%, 10%, 12%, 24%, and 26% (close to the liquid limit, 28%) to a compaction degree of 90%; it was difficult to compact the soil at a lower (< 8%) or a higher water content (> 26%). It can be seen from Fig. 11a that the PSD of compacted loess is bimodal even if molding water content is as low as 8%. In Fig. 11b, it shows that the specimen compacted at 24%, similar to the specimens compacted at 22%, has a trimodal PSD. However, when molding water content increases to 26%, the PSD is bimodal again.

This special change of the PSD shape could be attributed to that molding water content has a control on the occurrence of clay particles (Juang et al. 1986; Simms and Yanful 2002;
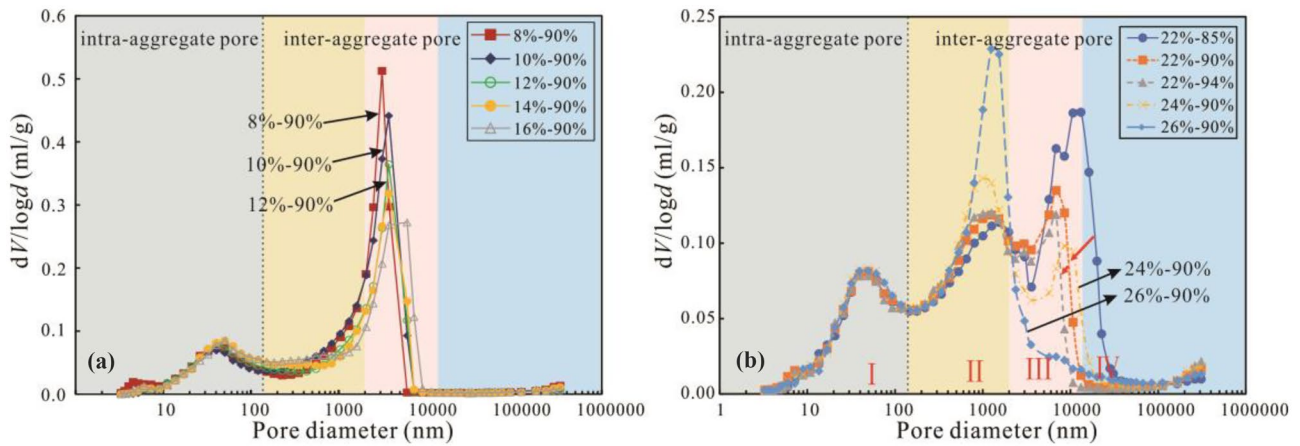
Fig. 11 PSDs of the specimens compacted at different water contents

Romero et al. 2011). There is a high tendency for clay aggregates to have large size at the dry side of the optimum since attractions are dominated between clay particles. However, at the wet side, electrostatic repulsion is produced since the electrostatic equilibrium in the DDL is destroyed by water molecules; meanwhile, osmotic repulsion between particles cannot be neglected. Both repulsions can lead to a reduction in the size of clay aggregates. So, the higher the molding water content, the smaller the size of clay aggregates. However, when there is a wide gap between the size of clay aggregates and that of silt aggregates (and clay-coated sands), the pores between clay aggregates could be the group of inter-aggregate pores with smaller diameter, while the pores between silt aggregates (and clay-coated sands) are the group of inter-aggregate pores with larger diameter. In other words, the PSD is trimodal, as shown in Fig. 11b; the peak in the range of small pores corresponds to the dominant diameter of the pores between clay aggregates, and the peak in the range of mesopores corresponds to the dominant diameter of the pores between silt aggregates (and clay-coated sands). With the further increase of molding water content (close to the liquid limit), the soil is nearly a paste, large pores could be filled with clay aggregates. As a result, there is only one group of inter-aggregate pores in the soil, the PSD becomes bimodal again.

The size distribution of intra-aggregate pores (or micro pores, ≤ 150 nm) remains unchanged no matter how molding water content changes. That is because aggregates are skeleton particles in compacted loess within the range of molding water content considered in this study (8–26%), the group of intra-aggregate pores (pores between clays in fact) cannot be changed as long as the clay content is unchanged. In other words, the size distribution and density of intra-aggregate pores in compacted loess are strongly dependent on the amount of clay (Juang et al. 1986) rather than molding water content (Hou et al. 2020).

4.2 Influence of the microstructure on the SWCC

The SWCC is the representation of interactions between solid particles and water stored in soil pores. It is widely recognized that there is a close relationship between the SWCC and PSD in the low suction range where the drainage of water is governed by the capillarity. The capillary law states an inverse relationship to the pore size being desaturated at a particular suction. Some classical SWCC models, such as Brooks and Corey model and Fredlund and Xing model, were obtained by integrating the function of PSD (Fredlund and Xing 1994). Experimental evidence indicates that soils with a dual-porosity structure, such as gap-graded soils, cracked soils, and fine-graded soils compacted at the dry side, may have a bimodal SWCC that can be considered as the superimposition of two unimodal SWCCs (Li et al. 2014). In other words, when two or more pore families exist in the soil, the SWCC might be bimodal or multimodal (Zhang and Chen 2005; Satyanaga et al. 2013). However, such a bimodal feature of the SWCC was not captured in this study. In fact, it is very difficult to obtain a bimodal SWCC, because it requires measuring the water contents at many suctions, which is very time-consuming; it also depends on the method or instrument used and the operator's ability and experience (Zapata et al. 2000). For this reason, the measured bimodal SWCC of loess (both intact loess and compacted loess) is rarely seen. In many studies on loess, the measured SWCCs are unimodal even though the samples tested have a dual-porosity structure along with a bimodal PSD (Muñoz-Castelblanco et al. 2012; Zhang et al. 2019; Hou et al. 2020; Wang et al. 2021). The first part of the bimodal SWCC measured by Ng et al. (2016) for a compacted loess is within the suction range of less than 20 kPa. So, a bimodal SWCC of compacted loess might be obtained by increasing the number of measurements in the range of 0 – 20 kPa.

Fig. 12 Relationship between the SWCC and PSD of compacted loess
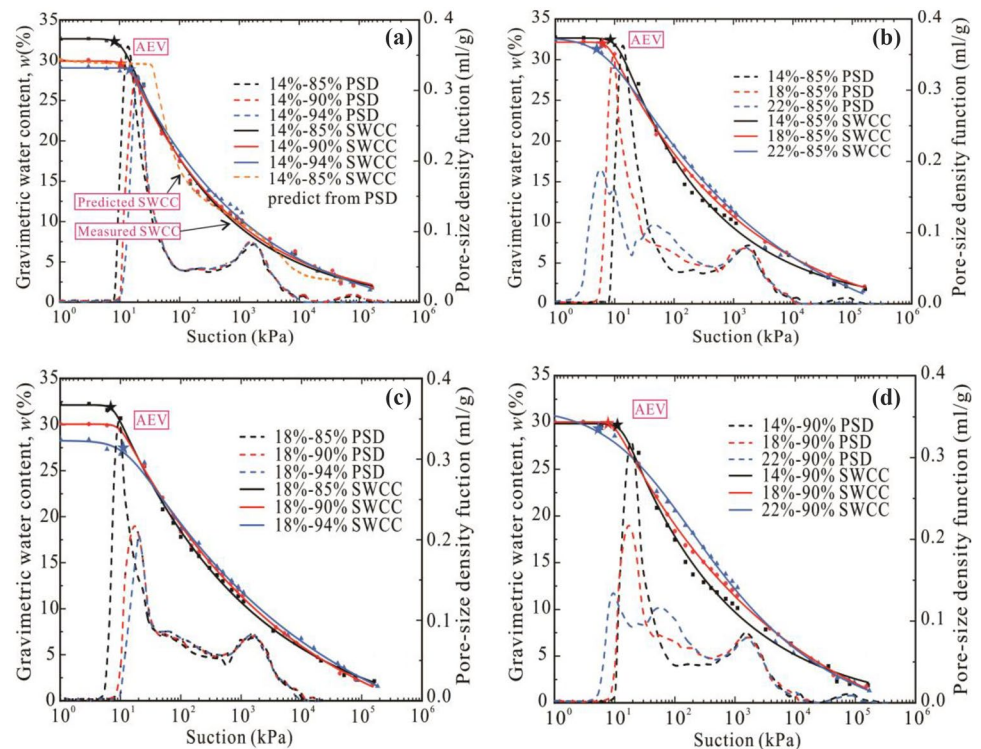

Figure 12 presents the measured SWCCs (including the data measured by pressure plate extractor and WP4C) and PSDs of some specimens (pore diameter is converted to suction according to the Yang-Laplace equation, $s = 2T_s\cos\alpha/r$, where s is the suction, T_s is the surface tension of water, α is the contact angle between solid particle and water, and r is the pore radius). The suctions converted from the pore sizes in the high suction range may not be the actual suctions since it is the adsorption that contributes to those suctions. This is also indicated by the inconsistency at high suctions (> 5000 kPa, approximately) between the measured SWCC and the SWCC predicted from the PSD (see Fig. 12a). It is worth mentioning that the predicted SWCC also does not match the measured SWCC at low suctions (< 100 kPa, approximately) (Fig. 12a). That is because, as mentioned before, pores with a diameter beyond the range of 3 nm–360 μm, insolated pores and constricted pores could not be detected by MIP. For this reason, the measured saturated water content is larger than that predicted from e_{in}. From Fig. 12, it can be seen that the AEV corresponds to a diameter at which there is a sharp increase in the pore-size density. Besides, the slope of SWCC in the transition zone is related to the range of dominant diameter of inter-aggregate pores; the narrower the range of dominant diameter, the steeper the SWCC in the transition zone (see Fig. 12b and d) that is consistent with the observation of Hou et al. (2020).

As a soil commences desaturating, air first replaces some of the water in large pores; in other words, water drains from large pores in response to suction increase in the low suction range, and vice versa. It can be seen from Fig. 12 that water drains from macropores and mesopores during the transition stage and from small pores and micropores during the residual stage. Since there are almost no macropores in the specimens (except for the specimen 22–85%), water drains mainly from mesopores during the transition stage. So, the higher the density of mesopores is, the more the water content decreases in the transition zone. Small pores and micropores have a control on the desiccation during the residual stage. For this reason, the specimens with different molding water contents have different PSDs in the ranges of mesopores and small pores (Fig. 7); they therefore have very different SWCCs in the transition zone and residual zone (Figs. 2 and 3). The specimens with different compaction degrees have different PSDs only in the range of mesopores; their SWCCs are close to each other in the residual zone (Fig. 12).

5 Conclusions

The PSDs and SWCCs of specimens with different molding water contents or compaction degrees were measured, to gain a deep insight into the effects of molding water content and compaction degree on the microstructure and water retention capacity of compacted loess. Several important conclusions can be drawn upon this integrated experimental study.

(1) The size distributions of small pores and mesopores are mainly different due to the difference in molding water content; at the same compaction degree, the higher the molding water content, the lower the density of mesopores, and the larger the density of small pores. However, at the same molding water content, mesopores are mainly affected and compressed from the larger to the smaller with the increase of compaction degree.

(2) Molding water content has a control on the size of aggregates in compacted loess; with the increase of molding water content, the size of aggregates (both clay aggregates and silt aggregates) decreases. When there is a wide gap between the size of clay aggregates and that of silt aggregates (and clay-coated sands), the PSD is trimodal, and there are two groups of inter-aggregates pores in the soil. As molding water content increases further (close to the liquid limit), large pores could be filled with clay aggregates; there is only one group of inter-aggregate pores in the soil, and the PSD becomes bimodal again.

(3) The influence of molding water content on the SWCC is mainly on the AEV and slope of the curve in the transition zone. At the same compaction degree, the specimen with a lower molding water content has a greater AEV and a larger slope of the curve in the transition zone. Compaction degree influences the AEV, and when presented in terms of gravimetric water content, the SWCCs are almost overlapped when suction is approximately greater than 30 kPa.

(4) Water drains mainly from mesopores during the transition stage and from small pores and micropores during the residual stage. There is a close relationship between the SWCC and PSD in the low suction range where the drainage of water is governed by the capillarity. The AEV corresponds to a diameter at which there is a sharp increase in the pore density. Besides, the specimen with a narrower range of dominant diameter of inter-aggregate pores has a larger slope of SWCC in the transition zone.

Declarations

Conflict of interest The authors declare no competing interests.

References

Aldaood A, Bouasker M, Al-Mukhtar M (2015) Soil-water characteristic curve of gypseous soil. Geotech Geol Eng 33:123–135

Al-Khazaali M, Vanapalli SK (2019) Experimental investigation of single model pile and pile group behavior in saturated and unsaturated sand. J Geotech Geoenviron Eng 145(12):0419112

Alonso EE, Pinyol NM, Gens A (2013) Compacted soil behaviour: initial state, structure and constitutive modelling. Géotechnique 63(6):463–478

Blatz JA, Graham J, Chandler NA (2002) Influence of suction on the strength and stiffness of compacted sand-bentonite. Can Geotech J 39(5):1005–1015

Casini F, Vaunat J, Romero E, Desideri A (2012) Consequences on water retention properties of double-porosity features in a compacted silt. Acta Geotech 7:139–150

Cheng Q, Tang CS, Zeng H, Zhu C, An N, Shi B (2020) Effects of microstructure on desiccation cracking of a compacted soil. Eng Geol 265:105418

Delage P, Audiguier M, Cui YJ, Howat M (1996) The micro-structure of a compacted silt. Can Geotech J 33:150–158

Derbyshire E (2001) Geological hazards in loess terrain, with particular reference to the loess regions of China. Earth Sci Rev 54:231–260

Fan W, Deng LS, Yuan WN (2017) Double parameter binary-medium model of fissured loess. Eng Geol 31(11):1752–1756

Fredlund DG, Xing A (1994) Equations for the soil-water characteristic curve. Can Geotech J 31(4):521–532

Fredlund DG, Rahardjo H, Fredlund MD (2012) Unsaturated soil mechanics in engineering practice. John Wiley & Sons. Hoboken, United States

Gallipoli D, Wheeler SJ, Karstunen M (2003) Modelling the variation of degree of saturation in a deformable unsaturated soil. Géotechnique 53:105–112

Ge MM, Pineda JA, Sheng DC, Burton GJ, Li N (2021) Microstructural effects on the wetting-induced collapse in compacted loess. Comput Geotech 138:104359

Guo Y, Ni WK, Kou Z, Zhao Y, Nie YP (2020) Experimental study on the permeability of compacted loess. Soil Mech Found Eng 57(5):394–400

Hou XK, Qi SW, Li TL, Guo SF, Wang Y, Li Y, Zhang LX (2020) Microstructure and soil-water retention behavior of compacted and intact silt loess. Eng Geol 277:105814

Hu R, Chen YF, Liu HH, Zhou CB (2013) A water retention curve and unsaturated hydraulic conductivity model for deformable soils: consideration of the change in pore-size distribution. Géotechnique 63:1389–1405

Jiang MJ, Zhang FG, Hu HJ, Cui YJ, Peng JB (2014) Structural characterization of natural loess and remolded loess under triaxial tests. Eng Geol 181:249–260

Jiang Y, Chen WW, Wang GH, Sun GP, Zhang FY (2017) Influence of initial dry density and water content on the soil-water characteristic curve and suction stress of a reconstituted loess soil. Bull Eng Geol Environ 76:1085–1095

John A, Fuentes HR, George F (2021) Characterization of the water retention curves of Everglades wetland soils. Geoderma 381:114724

Juang CH, Holtz RD (1986) Fabric, pore size distribution, and permeability of sandy soils. J Geotech Eng Div ASCE 112(9):855–868

Koliji A, Laloui L, Vulliet L (2009) Behaviour of unsaturated aggregated soil in oedometric condition. Soils Found 49(3):369–380

Kong LW, Guo AG (2011) Effect of water content on pore size distribution of red clay. Computer Methods for Geomechanics: Frontiers and New Applications 1: 523–527. https://doi.org/10.13140/RG.2.1.1899.0163

Li P, Vanapalli SK, Li TL (2016) Review of collapse triggering mechanism of collapsible soils due to wetting. J Rock Mech Geotech 8:256–274

Li P, Shao SJ, Vanapalli SK (2020) Characterizing and modeling the pore-size distribution evolution of a compacted loess during consolidation and shearing. J Soil Sediment 20:2855–2867

Li X, Li JH, Zhang LM (2014) Predicting bimodal soil–water characteristic curves and permeability functions using physically based parameters. Comput Geotech 57:85–96. https://doi.org/10.1016/j.compgeo.2014.01.004

Li XA, Li L, Song YH, Hong B, Wang L (2019) Characterization of the mechanisms underlying loess collapsibility for land-creation project in Shaanxi Province, China-a study from a micro perspective. Eng Geol 249:77–88

Lipovetsky T, Zhuang LW, Teixeira WG, Boyd A, May Pontedeiro E, Moriconi L, Alves JLD, Couto L, van Genuchten MT (2020) HYPROP measurements of the unsaturated hydraulic properties of a carbonate rock sample. J Hydrol 591:125706

Muñoz-Castelblanco JA, Pereira JM, Delage P, Cui YJ (2012) The water retention properties of a natural unsaturated loess from northern France. Géotechnique 62(2):95–106

Ng CWW, Sadeghi H, Hossen SB, Chiu CF, Alonso EE (2016) Water retention and volumetric characteristics of intact and recompacted loess. Can Geotech J 53:1258–1269

Patrick P, Olsen H, Higgins J (2007) Comparison of chilled-mirror measurements and filter paper estimates of total soil suction. Geotech Test J 30(5):1–8

Peng JB, Tong X, Wang SK, Ma PH (2018) Three-dimensional geological structures and sliding factors and modes of loess landslides. Environ Earth Sci 77:675

Rabot E, Wiesmeier M, Schlüter S, Vogel HJ (2018) Soil structure as an indicator of soil functions: a review. Geoderma 314:122–137

Romero E, Delia Vecchia G, Jommi C (2011) An insight into the water retention properties of compacted clayey soils. Géotechnique 61(4):313–328

Romero E, Gens A, Lloret A (1999) Water permeability, water retention, and microstructure of unsaturated compacted boom clay. Eng Geol 54(1–2):117–127

Satyanaga A, Rahardjo H, Leong EC, Wang JY (2013) Water characteristic curve of soil with bimodal grain-size distribution. Comput Geotech 48:51–61

Schelle H, Heise L, Jänicke K, Durner W (2013) Water retention characteristics of soils over the whole moisture range: a comparison of laboratory methods. Eur J Soil Sci 64(6):814–821

Shen JH, Hu MJ, Wang X, Zhang CY, Xu DS (2021) SWCC of calcareous silty sand under different fines contents and dry densities. Front Environ Sci 9:682907

Simms PH, Yanful EK (2002) Predicting soil-water characteristic curves of compacted plastic soils from measured pore-size distributions. Géotechnique 52(4):269–278

Sun DA, GaoY ZAN, Sheng DC (2016) Soil–water retention curves and microstructures of undisturbed and compacted Guilin lateritic clay. Bull Eng Geol Environ 75:781–791

van Genuchten MT (1980) A closed-form equation for predicting the hydraulic conductivity of unsaturated soils. Soil Sci Soc Am J 44(5):892–898

Vanapalli SK, Fredlund DG, Pufahl DE, Clifton AW (1996) Model for the prediction of shear strength with respect to soil suction. Can Geotech J 33(3):379–392

Vanapalli SK, Fredlund DG, Pufahl DE (1999) The influence of soil structure and stress history on the soil-water characteristics of a compacted till. Géotechnique 49:143–159

Wang JD, Li P, Ma Y, Vanapalli SK (2019) Evolution of pore-size distribution of intact loess and remolded loess due to consolidation. J Soil Sediment 19(3):1226–1238

Wang JD, Li P, Ma Y, Vanapalli SK, Wang XG (2020) Change in pore-size distribution of collapsible loess due to loading and inundating. Acta Geotech 15(5):1081–1094

Wang Y, Li TL, Zhao CX, Hou XK, Li P, Zhang YG (2021) A study on the effect of pore and particle distributions on the soil water characteristic curve of compacted loess soil. Environ Earth Sci 80:764

Wong JTF, Chen ZK, Chen XW, Ng CWW, Wong MH (2017) Soil-water retention behavior of compacted biochar-amended clay: a novel landfill final cover material. J Soil Sediment 17(3):1–9

Xiao T, Li P, Shao SJ (2022) Fractal dimension and its variation of intact and compacted loess. Powder Technol 395:476–490

Xu PP, Zhang QY, Qian H, Li MN, Yang FX (2021) An investigation into the relationship between saturated permeability and microstructure of remolded loess: a case study from Chinese Loess Plateau. Geoderma 382:114774

Zapata CE, Houston WN, Houston SL, Walsh KD (2000) Soil–water characteristic curve variability. Advances in Unsaturated Geotechnics. https://doi.org/10.1061/40510(287)7

Zhang FY, Zhao CX, Lourenço SDN, Dong S, Jiang Y (2021) Factors affecting the soil–water retention curve of Chinese loess. Bull Eng Geol Environ 80:717–729

Zhang LM, Chen Q (2005) Predicting bimodal soil-water characteristic curves. J Geotech Geoenviron 131(5):666–670

Zhang YW, Song ZP, Weng XL, Xie YL (2019) A new soil-water characteristic curve model for unsaturated loess based on wetting-induced pore deformation. Geofluids 2019:1–14

Zhu CH, Li N (2019) Ranking of influence factors and control technologies for the post-construction settlement of loess high-filling embankments. Comput Geotech 118:103320